Study of heat transfer in wood before the onset of pyrolysis at the cone calorimeter scale

Hassan Flity, Lucas Terrei, Zoubir Acem, Gilles Parent

International Journal of Thermal Sciences 210 (2025) 109545

Contents lists available at ScienceDirect

International Journal of Thermal Sciences

journal homepage: www.elsevier.com/locate/ijts

Study of heat transfer in wood before the onset of pyrolysis at the cone calorimeter scale

Hassan Flity, Lucas Terrei, Zoubir Acem, Gilles Parent *

Université de Lorraine, CNRS, LEMTA, F-54000, Nancy, France

ARTICLE INFO

Keywords:
Heat transfer in wood
Cone calorimeter
Anisotropy of wood thermal conductivity
Thermal properties of wood

ABSTRACT

This work is dedicated to the heat transfer in wood subjected to a heat flux equal to 4 $kW\,m^{-2}$. This heat flux was chosen so that the temperature of the wood did not exceed 200 °C, thus avoiding pyrolysis. In addition, the wood was oven-dried to avoid water evaporation. Under these conditions, only heat transfer takes place. The goal was to focus on heat transfer and to model it very finely. Experimentally, wood samples were exposed to the heat flux from the cone heater of a cone calorimeter. Twelve thin-wire thermocouples were embedded in the wood samples to provide access to the in-depth temperature, and the heat flux distribution was imaged using a thermal camera. Eight different wood species were investigated in this work. Numerically, a 3-dimensional heat transfer model was developed. The experimental non-uniform heat flux distribution was used for the radiative heat flux conditions, the thermal conductivity was considered anisotropic and variable with temperature, and convection was described by convective exchange coefficients. This heat transfer model was used as a direct model for an inverse method aimed at determining unknowns, namely the convective exchange coefficient and the variation with temperature of the thermal conductivity perpendicular to the wood fibers, which was described by a second order polynomial. The numerical results are in good agreement with the experimental data, realistic convective heat transfer coefficients have been obtained, and thermal conductivities estimated by the inverse method are very close to those determined by the parallel hot wire method. This demonstrates the reliability of the model, boundary conditions, and thermal properties used.

1. Introduction

Numerous studies have focused on the modeling of wood combustion *e.g.* [1–11]. This process is complex and involves several physical and chemical phenomena, including heat transfer, pyrolysis, char oxidation, drying, ignition, extinction and flame feedback. All of these phenomena interact with each other. For example, pyrolysis controls the amount of gases supporting the flame. At the same time, the flame and char oxidation provide an additional heat flux that induces more pyrolysis. Therefore, modeling these phenomena requires a highly complex multiphysical model involving a large number of processes that are not yet fully understood. To better handle these phenomena and facilitate their modeling, many studies have strategically isolated specific phenomena through different experimental approaches.

For instance, thermogravimetric analysis in an inert atmosphere allows the isolation of the pyrolysis phenomenon and the development of a kinetic model, as demonstrated by numerous studies *e.g.* [3,12–27]. Similarly, thermogravimetric analysis in an oxidative atmosphere, carried out on char samples, allows a focused study of the char oxidation phenomenon [28–32]. At a larger scale, specifically at the cone calorimeter scale, some studies have focused on the pyrolysis phenomena by conducting tests in atmosphere-controlled chambers [26,27,33,34] under various heat fluxes. Other studies have focused on ignition, or in other words, the onset of flame [35,36]. Such studies aimed to identify criteria for ignition, such as ignition temperature [33], critical ignition heat flux, and time to ignition, while varying parameters such as heat fluxes, moisture, wood species and cone orientation [37]. In addition, other studies have addressed the extinction phenomenon [38–41], specifically, to determine the critical mass loss rate and critical heat flux for flame extinction. Recently, Flity et al. [26] investigated heat transfer to estimate thermal boundary conditions at the cone calorimeter scale using a thermally inert material with well-known properties.

However, no study has specifically focused on heat transfer in virgin wood prior to the onset of pyrolysis, even though this phenomenon plays a key role in predicting the onset of local degradation and, consequently, the behavior of wood when exposed to fire. Indeed, pyrolysis is driven by how much heat comes to the pyrolysis zone from the exposed surface **and** by how much heat is drained by conduction in the virgin wood layer beyond the pyrolysis front. In addition,

* Corresponding author.
E-mail address: gilles.parent@univ-lorraine.fr (G. Parent).

https://doi.org/10.1016/j.ijthermalsci.2024.109545
Received 18 May 2024; Received in revised form 15 October 2024; Accepted 10 November 2024
Available online 6 December 2024

many assumptions are often made to simplify the boundary conditions (convective losses and incident radiative heat flux), but these have a significant impact on the results. In [42], it has been shown that the heat capacity depends only on temperature, while the thermal conductivity perpendicular to the fiber direction increases with density and temperature. Meanwhile, the thermal conductivity parallel to the fiber directions is almost independent of temperature and increases with density. The cone calorimeter is a very widely used tool in the fire science community for studying the fire behavior of materials. It provides a radiative heat flux up to about 100 $kW\,m^{-2}$ which is fairly homogeneous over a square area of 10 cm × 10 cm, which is the standard size of the samples studied with this apparatus. However, the homogeneity of the flux is far from perfect, as shown numerically in [43].

In the present work, the main challenge was to consider the non-uniformity of the incident heat flux, the anisotropy of the wood thermal conductivity and its dependence on temperature. To this end, experiments were performed using the cone heater of a cone calorimeter with a moderate heat flux so that the temperature remained low enough to prevent pyrolysis. In this way, heat transfer was isolated from the other phenomena, with the aim of accurately modeling heat transfer in virgin wood and validating that the wood thermal properties measured in [42] adequately characterize the wood. Accordingly, an experimental campaign was carried out on different wood species with a heat flux of 4 $kW\,m^{-2}$ to ensure that the temperature inside the wood samples did not exceed 200 °C, thus avoiding pyrolysis and charring. During these tests, a new technique was developed to map the heat flux received by the surface of a sample exposed to the cone and the obtained flux distribution was used in a 3-dimensional heat transfer model which was coded in Python®. This model was used to predict temperature changes inside a spruce sample exposed to 4 $kW\,m^{-2}$, measured at 21 different positions relative to the cone exposed surface and at 7 depths for each position. Finally, the model was applied to the thermograms for eight different wood species, to obtain convective heat coefficients and the wood thermal conductivities, the latter of which can be compared with values obtained from more direct measurements.

2. Materials and methods

In this work several oven-dried wood samples were tested with an imposed heat flux of 4 $kW\,m^{-2}$. This heat flux was chosen to ensure that the temperature inside the wood did not exceed 200 °C, thus allowing only heat transfer to occur. This section describes the experimental setup, the wood samples tested, and the temperature measurement technique used.

2.1. Wood species

Eight wood species were investigated in this study, namely ipe, beech, oak, larch, spruce, poplar, fir and balsa. Balsa, poplar, oak, beech, and ipe are classified as hardwoods, while fir, spruce, and larch are classified as softwoods. The choice of these particular species was based on either their widespread use or the desire to cover a wide range of densities, from 100 to 1000 $kg\,m^{-3}$.

2.2. Cone calorimeter

The cone calorimeter is a device used to study the thermal degradation and combustion of materials under different heat fluxes. Fig. 1 shows the experimental setup. The heat flux comes from an electrical heating resistor in the form of a conical coil, the temperature of which can be controlled. The sample to be tested is placed vertically and parallel to the heating coil at a distance of 25 mm to ensure to ensure a fairly uniform heat flux received at the surface. Depending on the temperature setting of the heater, the apparatus can provide heat fluxes between 0 and 100 $kW\,m^{-2}$. Before each test, the heat flux was checked

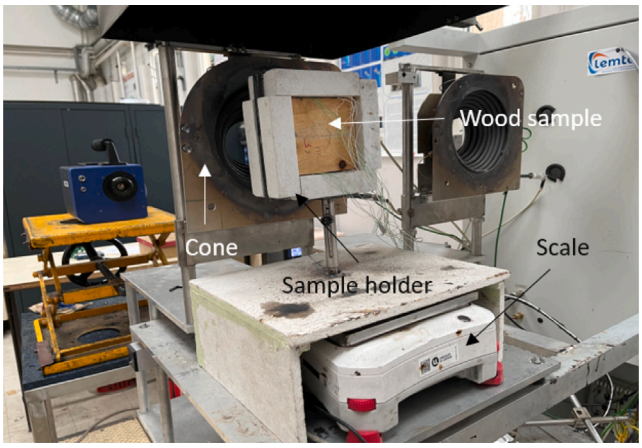

Fig. 1. Experimental setup of the cone calorimeter.

using a Schmidt-Boelter type flux meter (from Medtherm® company) positioned at the same height as the center of the exposed surface of the sample. In this work, the heat flux was maintained at 4 $kW\,m^{-2}$ and the cone was placed on a sliding table, which facilitates the installation of the sample prior to exposure to the heat flux and allows a very rapid transition from high flux to zero flux or vice versa [40].

2.3. Mass loss

The mass loss was measured with an OHAUS™ electronic weighing scale. This scale has a maximum capacity of 10200 g and an accuracy of 0.01 g and the acquisition frequency was set to 1 Hz. It was observed that no mass loss occurred during the experiments, confirming that no pyrolysis took place (nor water loss as the samples had been oven-dried).

2.4. In-depth temperature measurement

The internal temperature measurement technique developed by Terrei et al. [44] was used in this study. The implantation of thermocouples involves cutting the wood sample perpendicular to the exposed surface and machining square grooves of 0.2 mm at the desired locations. Position accuracy is evaluated as ±0.2 mm[1] Subsequently, K-type thermocouple wires with a 0.1 mm diameter were butt-welded and then inserted into the grooves. Finally, melamine-urea-formaldehyde (MUF) or resorcinol, depending on the wood species, was used to glue the two parts of the samples together. According to the supplier (TC Direc company), the K-type thermocouples used in this work have a ± 2.5 °C accuracy for temperatures below 333 °C, which corresponds to the temperature range reached in this study.

3. Homogeneity of the received heat flux

3.1. Experimental part

The aim of this section was to test the homogeneity of the incident heat flux. For this purpose, a spruce sample with a surface area of 10 × 10 cm^2 and a thickness of 5 cm was cut into 4 pieces: one piece with a width of 5 cm and three identical pieces with a width of 1.67 cm, as shown in Fig. 2(a). Fourteen thermocouples were implanted on each surface as shown in Fig. 2(b).

[1] Machining was performed with a manual milling machine without a digital readout. When checking the position of the grooves, there was a discrepancy between the desired positions (using the dial indicator) and the measured positions (using a caliper). This explains why the positions are not round values.

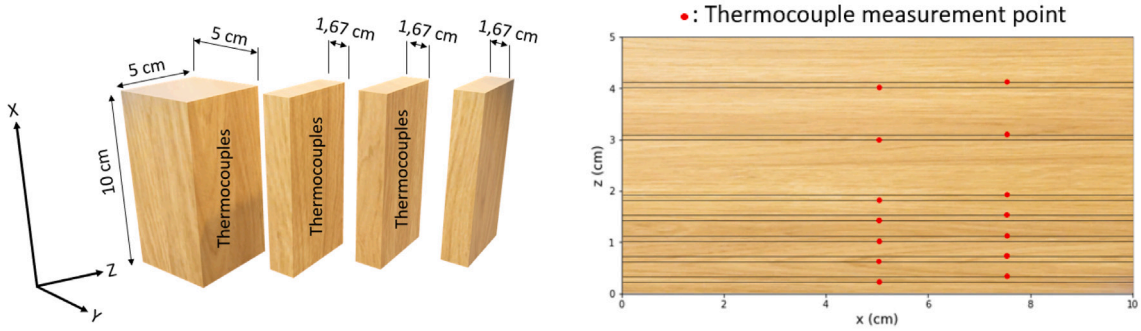

(a) Implantation surfaces. (b) Position of thermocouples.

Fig. 2. Implantation of 42 thermocouples in a spruce sample.

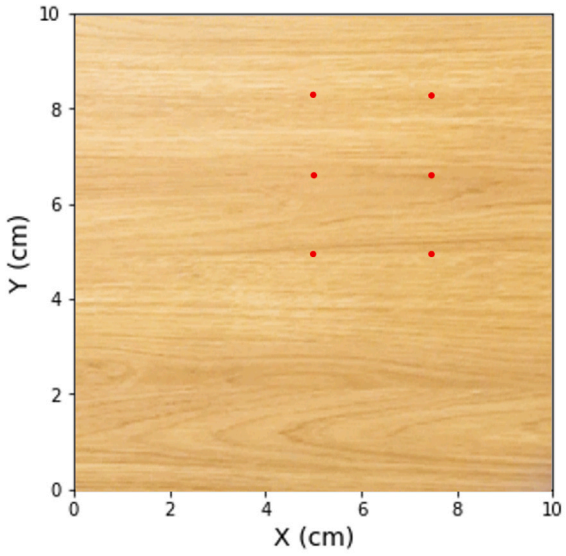

Fig. 3. Projection of the thermocouple positions on the (X, Y) plane, the plane exposed to the cone.

The pieces of the sample were then glued together. A total of 42 thermocouples were implanted in this sample. It was then dried in an oven at 105 °C for 48 h before testing. Fig. 3 shows the projection of the thermocouple positions on the (X, Y) plane, the plane exposed to the cone.

The temperatures given by the three thermocouples placed at depth of $z = 2.1$ mm (Fig. 4(a)) are shown in Fig. 4(b). These thermocouples were chosen because they are the closest to the surface exposed to the cone. It is noteworthy that the temperature reached by thermocouple 1, located in the center of the sample, is lower than that reached by thermocouple 3, located closer to the edge of the sample. If the radiative heat flux received by the sample and the convective losses were constant, the temperature at the center of the sample would have been the highest.

To further analyze the thermal behavior of the sample, four experiments were performed by exposing the same sample to the same 4 $kW\,m^{-2}$ heat flux. From one experiment to the next, the sample was rotated 90° clockwise from its previous orientation, as shown in Fig. 5. In this way, the temperature was measured at 21 different positions on the cone exposed surface and at seven depths for each position. Therefore, if temperature variations are observed using the same thermocouple when the sample is rotated 90°, this is likely due to heterogeneity of the heat flux and/or natural convection.

To assess the repeatability of the experiments, measurements from the thermocouple located at the center of the sample, (x, y, z) = (5 cm, 5 cm, 0.21 cm) were compared for the 4 experiments. This corresponds to thermocouple 1 shown in Fig. 4(a). This thermocouple remains in the same position when rotating the sample during the different experiments. Fig. 6(a) illustrates that the measurements of this thermocouple during the 4 experiments yield almost identical thermograms, with a maximum standard deviation of 1.9 °C. This underlines the reproducibility of the measurements.

Thermocouple 2, positioned at (x, y, z) = (5 cm, 6.67 cm, 0.21 cm) in experiment 1, is located at the position (x, y, z) = (6.67 cm, 5 cm, 0.21 cm) in experiment 2, at (x, y, z) = (5 cm, 3.33 cm, 0.21 cm) in experiment 3, and at (x, y, z) = (3.33 cm, 5 cm, 0.21 cm) in experiment 4. Fig. 6(b) displays the measurements of this thermocouple during the 4 experiments, and Fig. 6(c) shows the measurements of thermocouple 3, which was positioned at (x, y, z) = (5 cm, 8.33 cm, 0.21 cm) in experiment 1, throughout the 4 experiments.

Fig. 6 (b) and (c) show that, for a fixed depth (z = 0.21 cm), there are significant temperature differences depending on the position relative to the cone-exposed surface. This suggests that the observed variations in Fig. 4 are likely related to the non-uniformity of the incident heat flux or the natural convection Based on these results, it seemed important to perform a mapping of the incident flux.

3.2. Distribution of the heat flux

To assess the heat flux received at the sample surface, an infrared thermal camera was used. For this purpose, the camera does not look directly at the cone, a diffusing screen, placed at the same position as the sample is used. This screen was used in transmission because it is easier to place the camera behind the screen. A thin (1 mm thick) alumina plate was used as the screen as shown in Fig. 7. Alumina absorbs very little in the visible and infrared up to a wavelength of about 5 μm. A Telops MWE infrared camera was used. This camera operates in the mid-infrared range *i.e.* in the 1.5 – 5 μm spectral band, a range in which the alumina plate has a high transmission. The image obtained when the camera looks at the alumina plate is then proportional to the radiation heat flux distribution.

Fig. 8(a) shows the measured heat flux on a surface of 16 × 16 cm^2 (corresponding to the sample inside its insulating holder), located at a distance of 25 mm from the cone calorimeter, with a heat flux of 4 $kW\,m^{-2}$. It should be noted that the experiments with the sample with 42 thermocouples were performed without the sample holder, *i.e.* on a surface of 10 × 10 cm^2. Fig. 8(b), which is a reduction of Fig. 8(a), shows the distribution of the measured heat flux over a surface of 10 × 10 cm^2, corresponding to the wood sample only (excluding the sample holder). Fig. 8(b) shows that the heat flux distribution is not homogeneous and varies between 2.8 and 4.4 $kW\,m^{-2}$. It is worth noting that this heat flux is much lower than the usual heat fluxes used

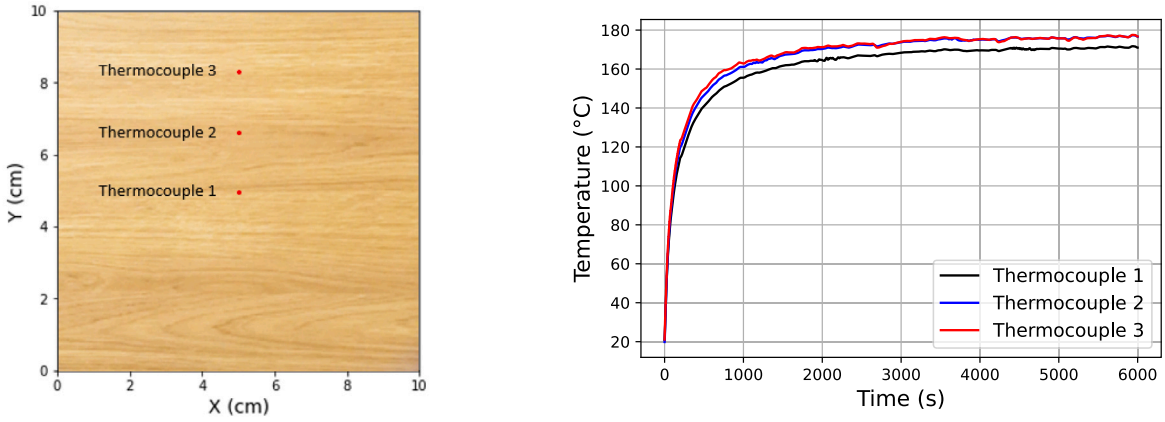

(a) Position of thermocouples. (b) Measured temperatures.

Fig. 4. Temperatures measured by the thermocouples placed at a depth of z = 0.2 cm.

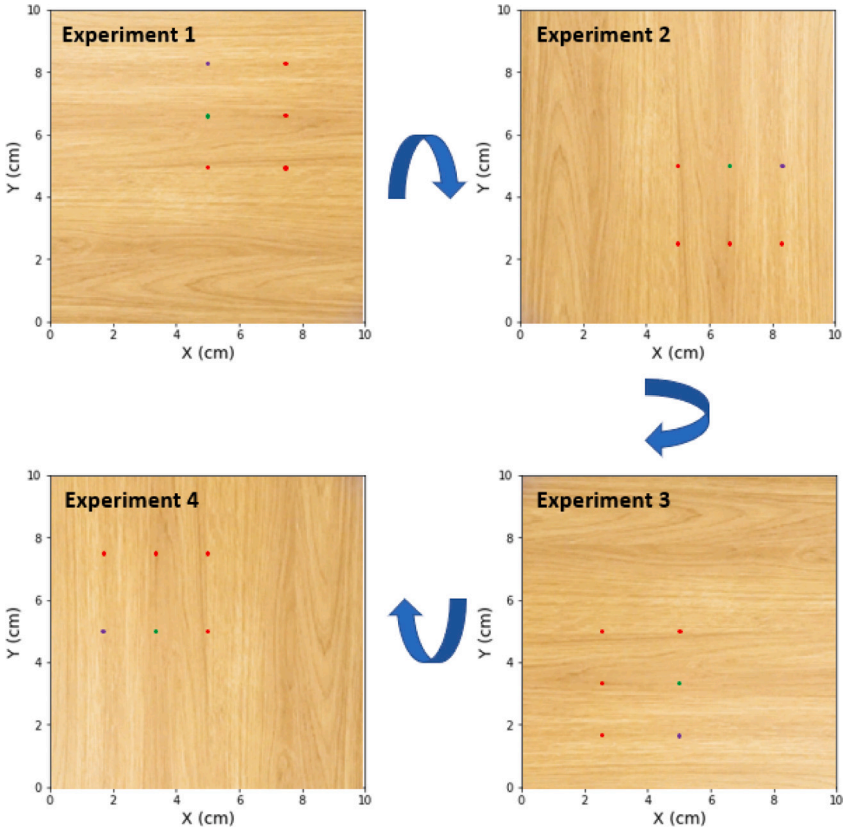

Fig. 5. Position of the thermocouples relative to the cone-exposed surface for each experiment.

with the cone calorimeter, so the heat flux could be more homogeneous at higher fluxes. This heat flux distribution partially explains the variations observed in the thermograms shown in Fig. 6. The measured heat flux distribution in this section was used as boundary condition in a heat transfer model to simulate the experiments performed in Section 3.1.

3.3. Numerical part

The purpose of this section was to model the experiments conducted on the spruce sample. The main objective of this work is to validate the measurements of the heat flux distribution of the cone, the thermal conductivity measurements in the directions perpendicular and parallel to the fibers which were performed in [42], and to determine the thermal boundary conditions for the tests at 4 $\mathrm{kW\,m^{-2}}$.

For this purpose, a finite volume method was used to solve numerically the heat transfer Eq. (1). An explicit scheme was used for the temporal discretization and the code was written in Python®.

$$\rho C_p(T)\frac{\partial T}{\partial t} = \nabla \cdot \left(\bar{\bar{\lambda}}_c(T)\nabla T\right) \tag{1}$$

ρ is the density of the spruce sample measured beforehand (357 $\mathrm{kg\,m^{-3}}$); $C_p(T)$ is the heat capacity of wood. The correlation given in [42] was used: $C_{p,\mathrm{wood}}(T) = 1131 + 4.67 \times (T - 273)$, where T is the temperature in Kelvin. It is based on calorimetric measurements made between room temperature and 95 °C. Above this temperature, $C_p(T)$ was extrapolated, which is reasonable since the results vary

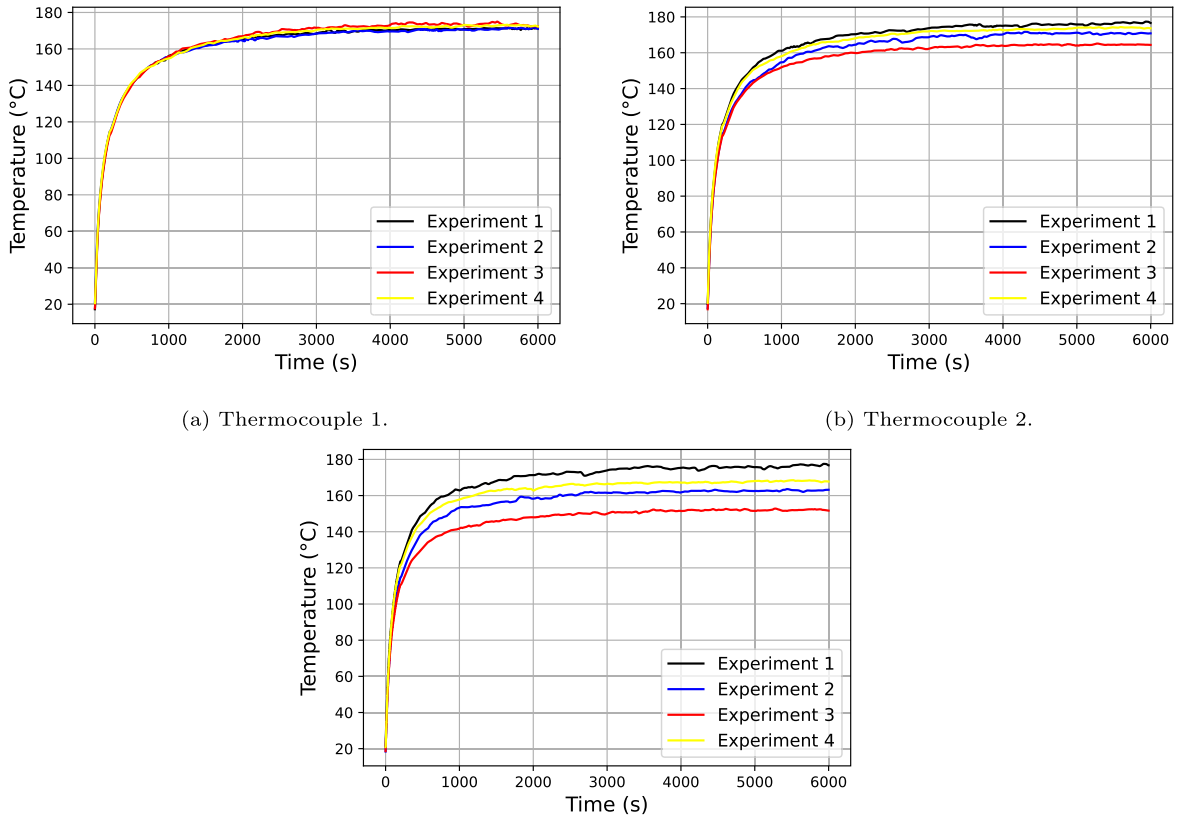

(a) Thermocouple 1.

(b) Thermocouple 2.

(c) Thermocouple 3.

Fig. 6. Temperatures measured by thermocouples 1, 2, and 3 illustrated in Fig. 4(a) between the different configurations shown in Fig. 5.

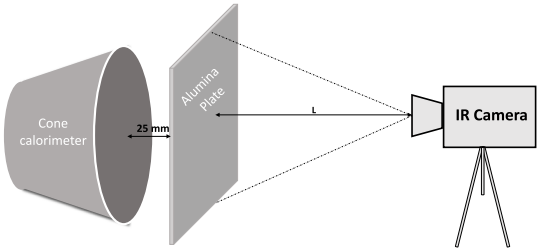

Fig. 7. Experimental set-up used to determine the distribution of the heat flux generated by the cone at a distance of 25 mm.

very linearly in the measurement temperature range. $\bar{\bar{\lambda}}_c$ is the thermal conductivity tensor expressed as:

$$\bar{\bar{\lambda}}_c = \begin{pmatrix} \lambda_{c\perp} & 0 & 0 \\ 0 & \lambda_{c\perp} & 0 \\ 0 & 0 & \lambda_{c\parallel} \end{pmatrix} \tag{2}$$

With $\lambda_{c\parallel}$ the conductivity in the direction parallel to the fibers: $\lambda_{c\parallel} = 8.4\times10^{-7}\times T^2 - 2.6\times10^{-4}\times T + 0.36$ W m^{-1} K^{-1}, where T is in °C, this correlation was obtained by fitting the hot-wire measurements for spruce wood presented in [42]. $\lambda_{c\perp}$ represents the conductivity in the direction perpendicular to the fibers and is assumed to vary according to a second-degree polynomial, with the coefficients to be determined by an inverse method. The boundary conditions are represented in Fig. 9.

"Flux" is the non-uniform heat flux distribution presented in Fig. 8(b); h_{front}, h_{rear}, and h_{lateral} are the convection coefficients for the front face, rear face, and lateral faces respectively; h_{lateral} is assumed to be the same for all four side faces. $T_{\text{S,front}}$, $T_{\text{S,rear}}$, and $T_{\text{S,lateral}}$ are the surface temperatures for the front face, rear face, and the four lateral faces respectively. $\alpha(T_{\text{cone}})$ is the wood absorptivity, which depends on the set point temperature of the cone. $\varepsilon(T_{\text{S,front}})$ is the emissivity, which depends on the surface temperature of the sample. T_a is the air temperature.

An inverse method was applied to all temperature measurements obtained from the four tests presented in Fig. 5, to extract the wood thermal conductivity and the convective exchange coefficients involved in the boundary conditions. From one test to another, the thermocouple positions changed (according to Fig. 5) as well as the fiber direction: for tests 1 and 3, the fiber direction is along the X direction; while, for tests 2 and 4, the fibers are along the Y direction. All other parameters remained the same. In total, the number of thermograms on which the inversion was performed is: 4 tests × 42 thermocouples = 168 thermograms. The Levenberg–Marquardt algorithm was used to minimize the squared differences between experimental and numerical temperatures (Eq. (3))

$$S = \sum_{i=1}^{N} \left[T_{\text{exp}}(t_i) - T_{\text{mod}}(t_i)\right]^2 \tag{3}$$

N is the number of points of the experimental thermograms, $T_{\text{mod}}(t_i)$ and $T_{\text{exp}}(t_i)$ are respectively the temperature computed by the 3D heat transfer model and the experimental temperature at time t_i.

The minimization was carried out to estimate h_{front}, h_{rear}, h_{lateral}, and the thermal conductivity of spruce. Although the latter was measured in [42], it was considered as unknown. Indeed, the recovery of a thermal conductivity that is close to the measured one is a good indicator of the reliability of the model and of the estimated parameters.

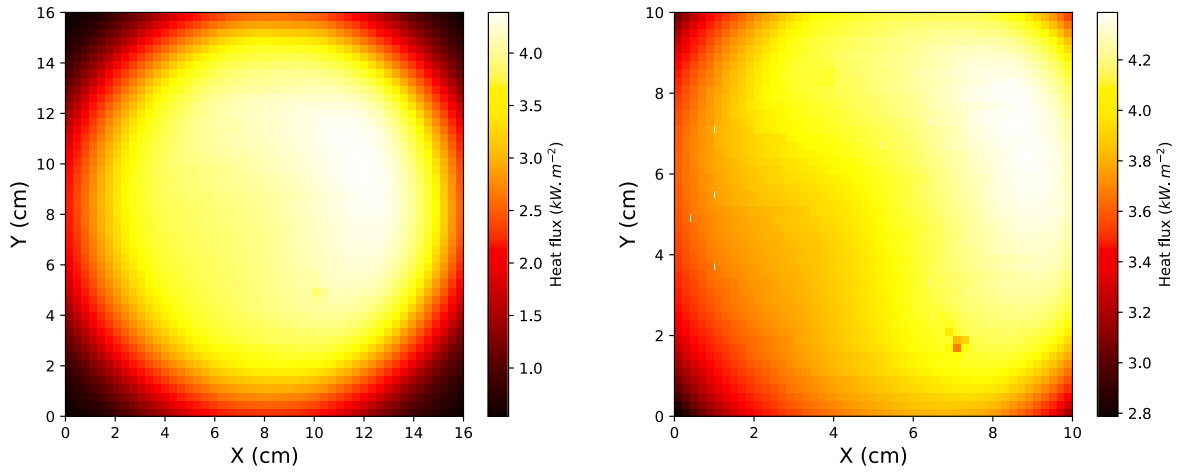

(a) 16 × 16 cm^2 (b) 10 × 10 cm^2

Fig. 8. Heat flux distribution on a 16 × 16 cm^2 surface (left) and 10 × 10 cm^2 (right), located at a distance of 25 mm from the cone calorimeter, for a heat flux of 4 kW m^{-2}.

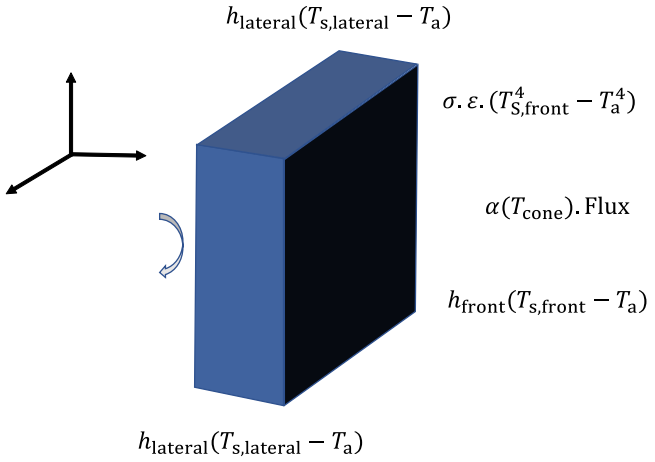

Fig. 9. Thermal boundary conditions.

3.4. Comparison between numerical and experimental results

Fig. 10 compares the numerical and experimental temperatures obtained for experiment 1 (Fig. 5) in the three planes: Y = 5 cm, Y = 6.67 cm and Y = 8.34 cm. Fig. 10(a) and (b) show that the numerical and experimental temperatures are in very good agreement for the thermocouples located in the two planes Y = 5 cm and Y = 6.67 cm. Regarding the thermocouples located in the Y = 8.34 cm plane, Fig. 10(c) shows that the numerical and experimental thermograms, located at position (X = 7.5, Y = 8.34) cm, match well. However, the experimental thermograms at position (X = 5, Y = 8.34) cm are slightly underestimated by the model. Appendix A presents the numerical and experimental temperatures obtained for the experiments 2, 3 and 4. In general, the model predicts the experimental temperatures well, and the heat flux distribution measured in the previous section appears to be reliable.

Fig. 11 presents the comparison between the thermal conductivity estimated by the inversion and the one measured using parallel the hot wire method in [42]. The average difference between the estimated and measured thermal conductivity is approximately 2.2%. This difference is lower than the uncertainty associated with the hot wire technique (10%). The convective heat transfer coefficients obtained are as follows: $h_{\text{front, heating}}$ = 9.5 W m^{-2} K^{-1}. h_{rear} = 3.5 W m^{-2} K^{-1} and h_{lateral} = 6.5 W m^{-2} K^{-1}.

In order to assess the impact of the non-homogeneity of the heat flux and the anisotropy of the wood, three additional simulations were performed using the heat transfer model. In the first simulation, all parameters were kept the same, except for the heat flux, which was assumed to be uniform over the entire surface of the sample exposed to the cone. In the second simulation, all parameters were kept the same, except for the conductivity tensor. Specifically, the conductivity parallel to the fibers was assumed to be equal to the conductivity perpendicular to the fibers, *i.e.* wood was considered isotropic in this simulation. The third simulation was performed with a 1D heat transfer model. The mean square errors obtained are 4.4 °C, 4.8 °C, and 6.4 °C for simulations 1, 2 and 3, respectively. Taking into account the heterogeneity of the heat flux and the anisotropy of wood (*i.e.* the most complete simulation presented above), the mean square error is only 3.2 °C. This demonstrates the improvement achieved by considering both the wood anisotropy and the heterogeneity of the heat flux distribution in the model.

4. Study at 4 kW m^{-2} for all wood species

After a thorough study of the heat transfer in the spruce sample instrumented with 42 thermocouples and demonstrating the effectiveness of the developed 3D model, it was applied to tests conducted on other wood species instrumented with 12 thermocouples placed in the center of the samples. The tests performed are first described, followed by their modeling.

4.1. Experimental part

All wood species were tested at a heat flux of 4 kW m^{-2}. The wood samples with dimensions of 10 × 10 cm^2 were dried in an oven at 105 °C for 48 h to remove moisture and thus limit the phenomena to heat transfer only. No mass loss was observed during the tests, confirming it was the case. A sample holder made of Silcal 1100® (low density calcium silicate) was used to minimize heat loss at the sides of the sample.

Temperatures inside the samples were measured by embedded thermocouples located in the center of the wood sample at various depths: 2.1, 4.1, 6.2, 8.3, 10.3, 12.4, 14.5, 16.6, 18.6, 20.7, 31.0, and 41.4 mm. During the tests, the sliding cone allowed to monitor the temperature evolution during heating (exposure of the sample to the cone) as well as during cooling (sliding of the cone and exposure of the sample to zero heat flux). For each wood species, five tests were performed on different samples.

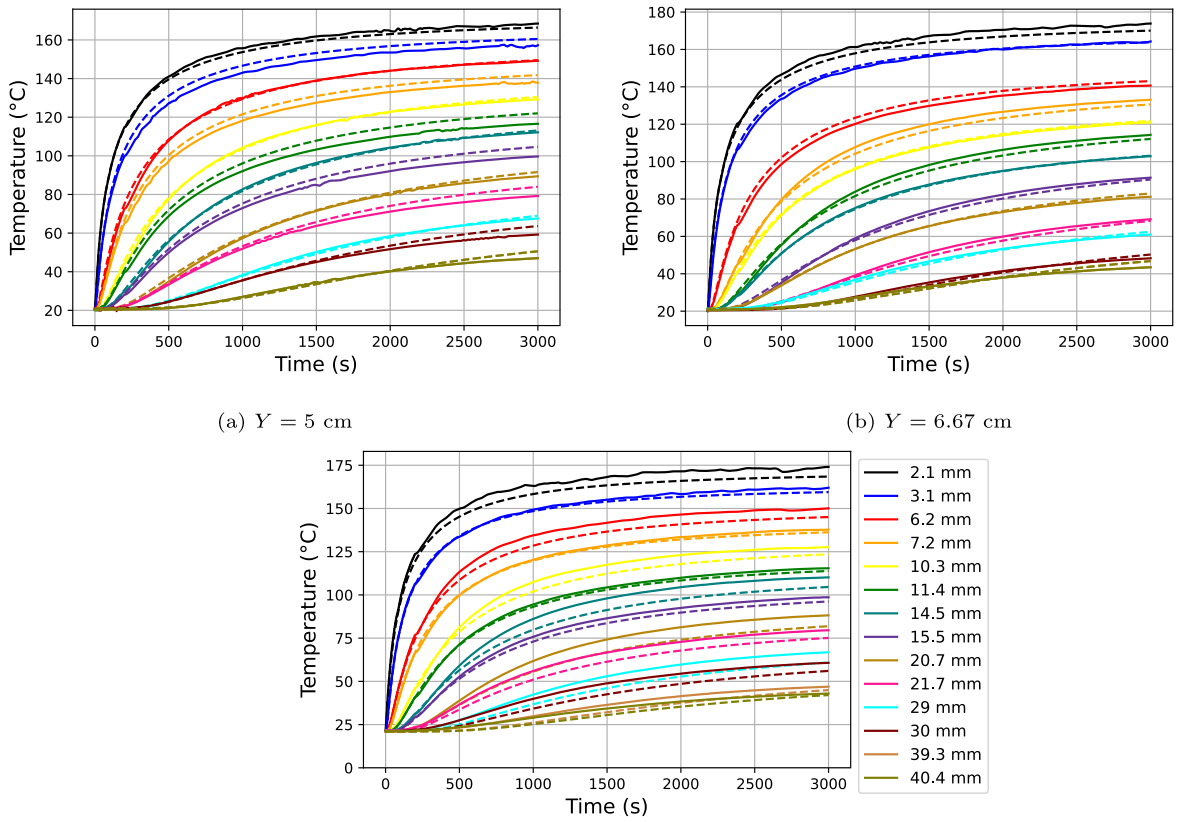

Fig. 10. Comparison of the numerical and experimental temperatures obtained for experiment 1, as shown in Fig. 5.

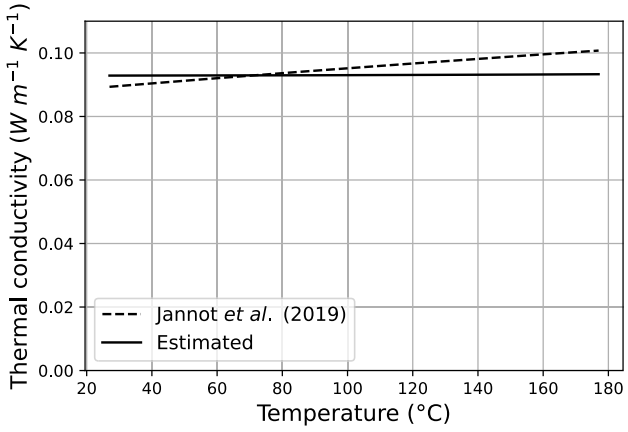

Fig. 11. Thermal conductivity of spruce estimated by the inverse method (present work) and measured using the hot wire method (ref [45]).

4.2. Numerical part

The heat transfer model, described in Section 3.3, was used to simulate the tests conducted on all wood species with a heat flux of 4 $\mathrm{kW\,m^{-2}}$, using the same boundary conditions shown in Fig. 9.

The sample holder was made of calcium silicate (Silcal 1100®). Its density was 240 $\mathrm{kg\,m^{-3}}$, and it was considered as an isotropic material. Its specific heat and thermal conductivity were measured between 150 and 900 °C using the parallel hot wire method described in [45]. The variations of specific heat and thermal conductivity with temperature are given by the following equations:

$$C_p(T) = 439 + \times 83 \log_{10}(T) \tag{4}$$

$$\lambda(T) = 4.1 \times 10^{-8}(T-273)^2 + 7.8 \times 10^{-5}(T-273) + 8.1 \times 10^{-2} \tag{5}$$

where T is the temperature in Kelvin. Absorptivity and emissivity of calcium silicate were obtained from spectral reflectivity measurements. More details are provided in Appendix B. The variation of the average emissivity as a function of the temperature is given by the following equation:

$$\bar{\varepsilon}(T) = -1.16 \times 10^{-7} T^2 + 4.26 \times 10^{-6} T + 0.99 \tag{6}$$

where T is the surface temperature of the calcium silicate. The average absorptivity can also be calculated using Eq. (6) with T corresponding to the cone temperature (the radiating body). Perfect thermal contact was assumed between the calcium silicate holder and the wood sample.

The wood thermal properties vary from one species to the other. They were determined as follows:

- The density was measured for each sample.
- The absorptivity and emissivity used in the model are presented in Fig. 12. As for calcium silicate, these properties were obtained from spectral reflectivity measurements (see Appendix B). Balsa has the lowest emissivity and absorptivity, which is consistent with it being the whitest in the visible, followed by poplar which also has a light color. Ipe, which is the darkest type of wood, also has the highest emissivity/absorptivity. These two quantities are large (minimum value 0.85) because Planck's function, which is used to calculate the average values (see Eqs. (B.1) and (B.2)), is mainly located in the infrared range where wood has a large spectral absorptivity, see Fig. B.18. The emissivity of wood decreases

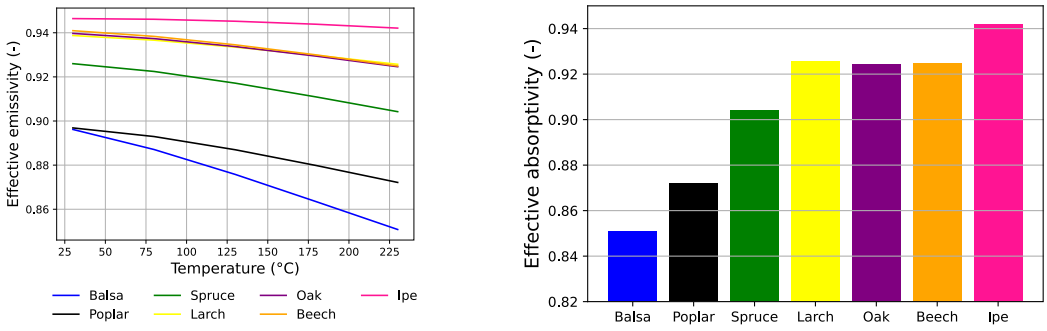

(a) Emissivity (b) Absorptivity

Fig. 12. Variation of wood emissivity with temperature, and absorptivity of the studied wood species.

slightly with temperature because Planck's function shifts toward short wavelengths, where the spectral emissivity of wood is lower, as temperature increases (Wien's law). It is worth noting that since there is no pyrolysis, the spectral absorptivity/emissivity is kept the same throughout the experiments.

- For each wood species, the thermal conductivity parallel to the fibers was assumed to be temperature-independent and equal to the average of values measured using the hot wire method at different temperatures. Thus, the conductivity values parallel to the fibers used in the model are as follows: 0.134, 0.298, 0.34, 0.47, 0.51, and 0.63 $\mathrm{W\,m^{-1}\,K^{-1}}$ for balsa, poplar, spruce, larch, oak, beech, and ipe, respectively. It is worth noting that since the temperature gradient parallel to the sample surface is small, the heat transfer is little dependent on this component of the thermal conductivity tensor.
- The thermal conductivity perpendicular to the fibers was assumed to vary with temperature according to a second-degree polynomial whose coefficients have to be estimated by the inverse method for each wood species.
- For all wood species, the heat capacity of wood was assumed to follow the same linear law with temperature as for spruce, *i.e.* $C_{p,\mathrm{wood}}(T) = 1131 + 4.67 \times (T - 273)$, where T is in K. Indeed, it has been shown in [42] that this property does not depend on the wood species.

For each test, the thermograms were used as data for the inverse method. The parameters to be estimated are h_{front}, h_{rear}, and the coefficients of the polynomial describing the thermal conductivity perpendicular to the fibers. h_{lateral} was fixed at 10 $\mathrm{W\,m^{-2}\,K^{-1}}$ since temperatures measured in the middle of the sample are not sensitive to this coefficient. It was assumed that h_{front} during heating could be different from that during cooling. It should be noted that $h_{\mathrm{front,\ heating}}$ and $h_{\mathrm{front,\ cooling}}$ are the convection coefficients of the face exposed to the cone during the heating and cooling phases, respectively. The 3-dimensional heat transfer model with the non-uniform heat flux described herein above was used as direct model for the inversion, and the Levenberg–Marquardt algorithm was utilized to minimize the squared differences between experimental and computed temperatures (Eq. (3)).

4.3. Comparison of numerical and experimental results

Fig. 13 shows experimental and numerical temperatures for one of the five tests for each wood species For each test, the sample was exposed to the cone for approximately two hours and then the exposure was interrupted by sliding the cone, allowing both heating and cooling of the wood sample to be studied.

Fig. 13 shows that the experimental thermograms follow the same trend regardless of the wood species. During heating, the temperatures within the sample gradually increase until reaching plateaus. After almost two hours, the heat source is removed, the cooling begins and the temperatures decrease quasi-exponentially. Fig. 13 also demonstrates that experimental and numerical thermograms comply very well regardless of the wood species. The Root Mean Square Errors (RMSE) were between 0.7 and 2.6 °C for all wood species, corresponding to a Normalized Root Mean Square Error (NRMSE) less than 1% for all species, except for larch, for which the NRMSE was 1.6%.

Fig. 14 presents a comparison between the thermal conductivities estimated by the inversion of the thermograms and those measured with the hot-wire method in [42] for all wood species. The conductivity measured by the hot-wire method, shown in Fig. 14, is the average of the five conductivities obtained by using the sample density in the following equation:

$$\lambda_{\perp} = 0.0386 + 0.1708 \times \frac{\rho_{\mathrm{dry}}}{\rho_{\mathrm{max}}} \times \sqrt{\frac{T}{T_{\mathrm{max}}}} \tag{7}$$

Where : $\rho_{\mathrm{max}} = 1000\ \mathrm{kg\,m^{-3}}$ and $T_{\mathrm{max}} = 433$ K. The correlation presented in Eq. (7) was established by adjusting the conductivity measurements obtained by the hot-wire method in the direction perpendicular to the fibers in [42]. Similarly, the average of the five conductivities obtained by the inversion of the thermograms is also shown for each wood species. The standard deviations of the five tests are also shown in Fig. 14 (red colored bands).

Fig. 14 shows that the conductivities estimated using the inversion method are close to those obtained using the parallel hot-wire method. Indeed, the average differences between the estimated and measured thermal conductivity for balsa (8.1%), poplar (7.6%), oak (3%), beech (1.6%), and ipe (2.3%) are even lower than the measurement uncertainty of the hot-wire technique (10%). The average differences between the two conductivities are higher for spruce (12.7%) and larch (19.6%). These differences may be related to the assumption of considering an homogeneous and isotropic conductivity in the plane perpendicular to the wood fibers (whereas tangential and radial conductivities can be different). This assumption was made both in the modeling (Section 3.3) and in the hot-wire measurements. It seems that the assumption of an effective isotropic conductivity in the plane perpendicular to the fibers is more relevant for hardwood species than for softwood species (we note that annual rings are usually more pronounced in softwood than in hardwood, and particularly in larch). Nevertheless, a deviation of 12% and 19% remains really reasonable.

Table 1 presents the convection coefficients estimated by the inversion method for all wood species. These are the mean values calculated from five tests, and the standard deviations (σ) are also indicated in the table. The model assumes a convection coefficient for the surface exposed to the cone which is not the same during the cooling phase and the heating phase. Table 1 shows that the convection coefficient for the surface exposed to the cone $h_{\mathrm{front,\ heating}}$ is similar for all wood species. Furthermore, the calculated standard deviations for this coefficient

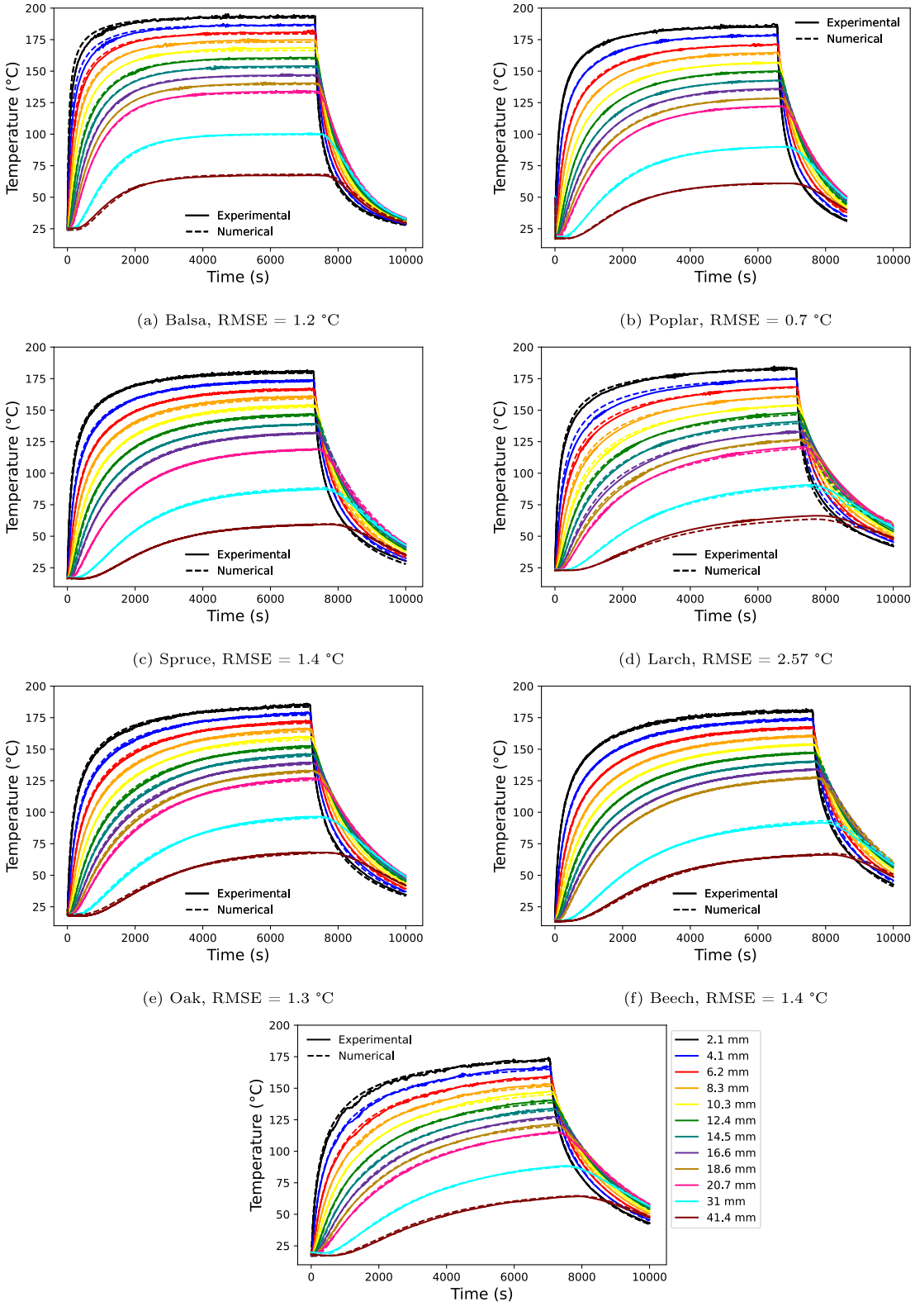

(a) Balsa, RMSE = 1.2 °C

(b) Poplar, RMSE = 0.7 °C

(c) Spruce, RMSE = 1.4 °C

(d) Larch, RMSE = 2.57 °C

(e) Oak, RMSE = 1.3 °C

(f) Beech, RMSE = 1.4 °C

(g) Ipe, RMSE = 1.1 °C

Fig. 13. Comparison between experimental and numerical temperatures inside samples of different wood species at 4 $kW\,m^{-2}$.

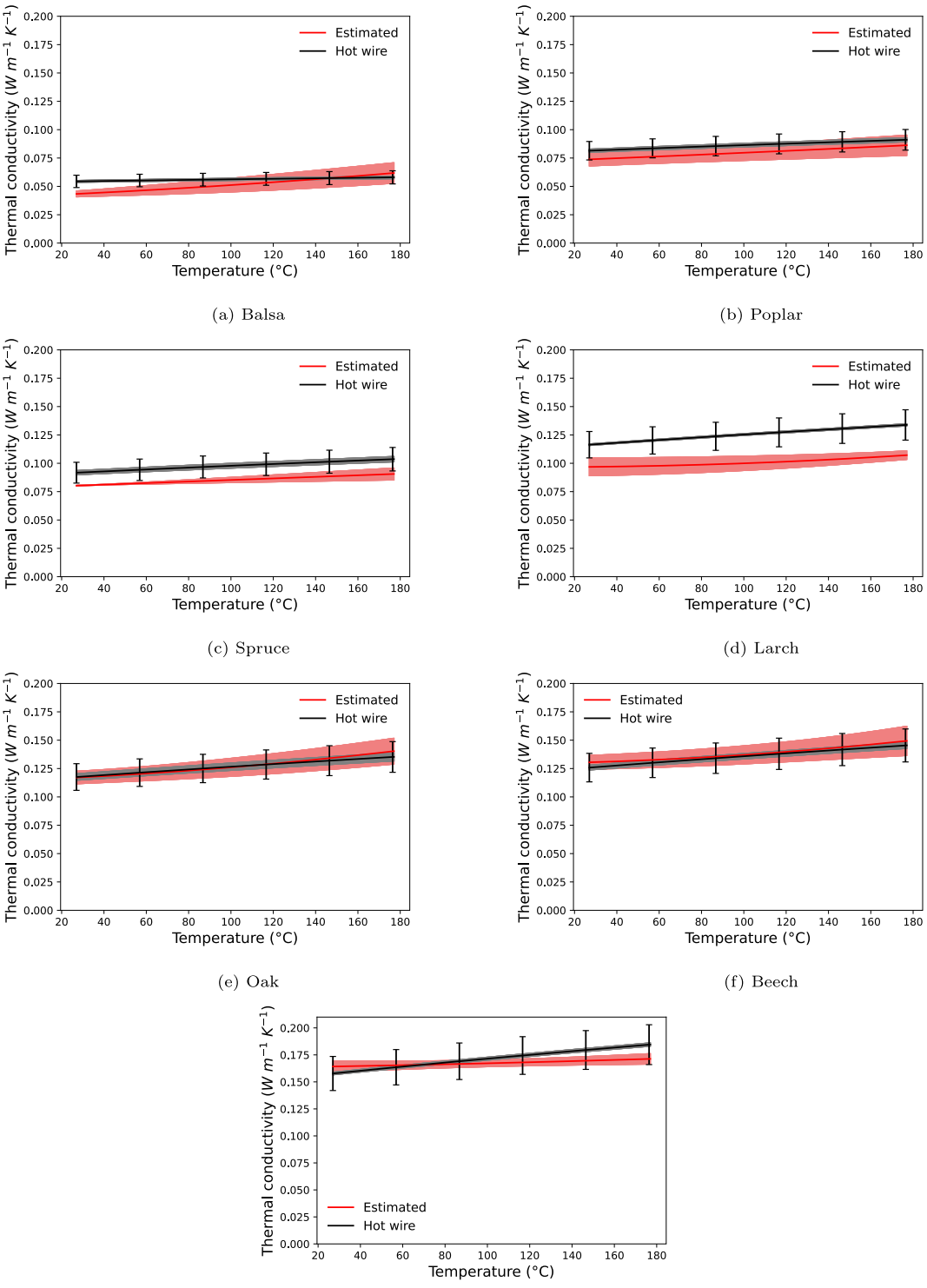

Fig. 14. Comparison between the estimated and measured thermal conductivities for different wood species. The red colored band corresponds to the standard deviation of five different tests and the black error bars correspond to the 10% uncertainty of the hot wire method.

are small, indicating that this coefficient does not vary significantly from one test to another for the same wood species. In general, the magnitude of this coefficient is quite close to the values calculated by natural convection correlations, which reinforces the reliability of the obtained results.

The convection coefficient $h_{\text{front, cooling}}$ varies between 4.3 and 7.4 $\text{W m}^{-2}\,\text{K}^{-1}$. These values are slightly lower than those of $h_{\text{front, heating}}$. This difference can be attributed to the fact that convective losses depend on the air temperature. In the heating phase, the air temperature is higher than during cooling. Therefore, since the model considers the

Table 1
Estimated convection coefficients for all wood species.

Species	$h_{\text{front, heating}}$ $\pm\ \sigma$ ($\mathrm{W\,m^{-2}\,K^{-1}}$)	$h_{\text{front, cooling}}$ $\pm\ \sigma$ ($\mathrm{W\,m^{-2}\,K^{-1}}$)	h_{rear} $\pm\ \sigma$ ($\mathrm{W\,m^{-2}\,K^{-1}}$)
Balsa	8.4 ± 0.3	5.7 ± 0.5	13 ± 1.5
Poplar	7.1 ± 0.6	7.4 ± 1.4	14.6 ± 3.2
Spruce	6.9 ± 0.3	4.9 ± 1	10 ± 2.2
Larch	6.5 ± 0.3	5.8 ± 0.5	14.5 ± 1.9
Oak	7.1 ± 0.4	4.3 ± 0.5	12.2 ± 2
Beech	8.1 ± 1	5.8 ± 0.9	11.7 ± 2.6
Ipe	6.9 ± 0.5	6.7 ± 0.9	14 ± 2

same air temperature for both phases, it is logical to obtain slightly lower values for $h_{\text{front, cooling}}$ compared to $h_{\text{front, heating}}$.

For the rear surface, the convection coefficients vary between 10 and 15 $\mathrm{W\,m^{-2}\,K^{-1}}$. These values are slightly higher than those calculated by natural convection correlations. In addition, the standard deviations are larger than for the other coefficients. The inversion was performed using thermograms at the twelve depths. This means that the inversion relies on measurements much closer to the surface exposed to the cone, making the data more sensitive to the convection coefficient of the surface exposed to the cone compared to the rear surface of the sample. Therefore, it is not surprising to obtain more reliable results for the surface exposed to the cone than for the rear surface of the sample.

5. Conclusion

In this paper, the study of heat transfer during cone calorimeter tests prior to the onset of pyrolysis was conducted with the aim of validating the thermal properties measured in a previous work [42] and modeling heat transfer in wood. An experimental campaign was carried out on various dry wood species with a heat flux of 4 $\mathrm{kW\,m^{-2}}$ chosen to ensure that the temperature inside the wood samples did not exceed 200 °C, thus avoiding pyrolysis and char oxidation reactions, that was confirmed by the absence of mass loss during the experiment.

During these tests, special attention was paid to the study of the non-homogeneity of the heat flux received by the sample. A new technique was developed to map the heat flux received by the surface of a sample exposed to the cone. In this technique, a thin alumina plate was exposed to the cone calorimeter. This plate acted as a screen, allowing the irradiance received on it to be observed by an infrared camera looking at the back surface of the plate. The choice of alumina was based on its diffusing nature and its high transmittance in the mid infrared. This technique is particularly interesting because it allows a complete map of the radiant heat flux distribution to be obtained from a single image in the infrared.

This map was used in a 3-dimensional heat transfer model. This model was able to predict temperature changes measured at 21 different positions relative to the cone-exposed surface and at 7 depths for each position.

Finally, an inverse method was applied to the temperature measured in tests performed at 4 $\mathrm{kW\,m^{-2}}$ with seven different wood species to estimate thermal conductivity of wood perpendicular to the fibers and the thermal boundary conditions. The results led to numerical thermograms in excellent agreement with the experimental thermograms. Moreover, the conductivity values obtained for the various wood species were close to the conductivity values measured by the hot wire method. It can also be emphasized that the wood heat capacity above 95 °C was not measured but extrapolated. The very good agreement between experimental and numerical results gives confidence in the validity of this assumption. Finally, the values of convective heat transfer coefficient were close to the values derived from natural convection correlations. All these results are reassuring regarding the reliability of the hot wire measurements, the measured heat flux distribution, the developed model, and the chosen boundary conditions.

CRediT authorship contribution statement

Hassan Flity: Writing – original draft, Visualization, Software, Investigation, Formal analysis, Data curation. **Lucas Terrei:** Writing – review & editing, Visualization, Formal analysis, Data curation. **Zoubir Acem:** Writing – review & editing, Supervision, Conceptualization. **Gilles Parent:** Writing – review & editing, Writing – original draft, Supervision, Funding acquisition, Conceptualization.

Acknowledgment

The measurements carried out in this work were made on the Métro'NRJ metrology platform at Université de Lorraine.

Declaration of competing interest

The authors declare that they have no known competing financial interests or personal relationships that could have appeared to influence the work reported in this paper.

Appendix A

See Figs. A.15–A.17.

Appendix B

A Fourier-transform infrared spectrometer was used to measure the emissivity and absorptivity of all samples. This is an indirect measurement. Indeed, the hemispherical directional spectral reflectance R_λ was characterized over a spectral range from 450 to 20 000 $\mathrm{cm^{-1}}$ (corresponding to a wavelength range of 0.5 µm – 22.2 µm). Assuming that wood is opaque, the spectral absorptivity α_λ is deduced by: $\alpha_\lambda = 1 - R_\lambda$. The spectral emissivity ε_λ is equal to the spectral absorptivity according to Kirchhoff's law. Fig. B.18 shows the spectral absorptivities for the different wood species.

Based on these measurements, the average absorptivity ($\overline{\alpha}$) and emissivity ($\overline{\varepsilon}$) are calculated using the Planck average:

$$\overline{\alpha}\left(T_{\text{cone}}\right) = \frac{\int_{0.5}^{22} \alpha_\lambda\left(\lambda_L\right) I_{\text{bb}}\left(\lambda_L, T_{\text{cone}}\right) d\lambda_L}{\int_{.5}^{22} I_{\text{bb}}\left(\lambda_L, T_{\text{cone}}\right) d\lambda_L} \tag{B.1}$$

$$\overline{\varepsilon}\left(T_{\text{surface}}\right) = \frac{\int_{0.5}^{22} \varepsilon_\lambda\left(\lambda_L\right) I_{\text{bb}}\left(\lambda_L, T_{\text{surface}}\right) d\lambda_L}{\int_{0.5}^{22} I_{\text{bb}}\left(\lambda_L, T_{\text{surface}}\right) d\lambda_L} \tag{B.2}$$

where: T_{cone} is the temperature of the radiating body, which is the calorimeter cone in this study (assuming the calorimeter cone emits radiation close to that of a black body); T_{surface} is the temperature of the wood emitting surface for which we want to calculate the emissivity; λ_L is the wavelength, and $I_{\text{bb}}\left(\lambda_L, T_{\text{surface}}\right)$ is the spectral intensity of the black body (Planck's function) expressed by:

$$I_{\text{bb}}\left(\lambda, T\right) = \frac{2h_p c^2 \lambda_L^{-5}}{\exp\left(\frac{h_p c}{\lambda_L T k_B}\right) - 1} \tag{B.3}$$

where h_p, c, and k_B are respectively the Planck constant, the speed of light, and the Boltzmann constant, and T represents either the temperature of the cone for the calculation of absorptivity or the temperature of the wood surface for the calculation of emissivity.

Data availability

Data will be made available on request.

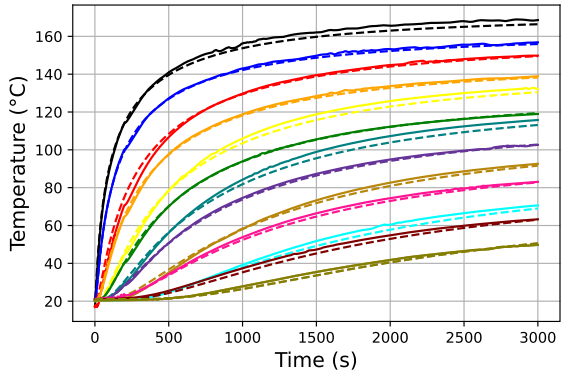

(a) $X = 5$ cm

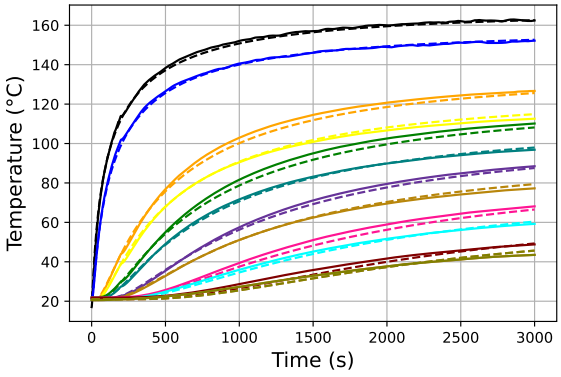

(b) $X = 6,67$ cm

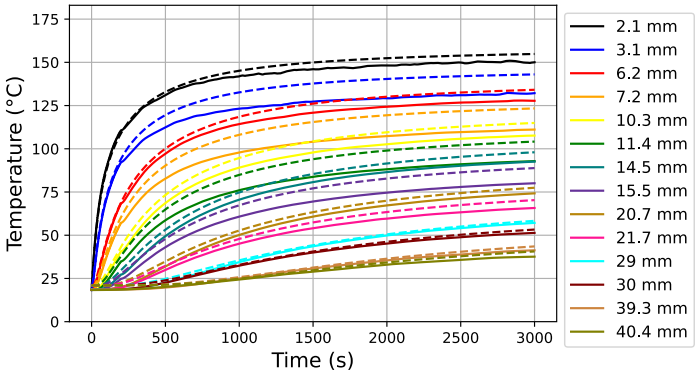

(c) $X = 8,34$ cm

Fig. A.15. Comparison of the numerical and experimental temperatures obtained for experiment 2, presented in Fig. 5.

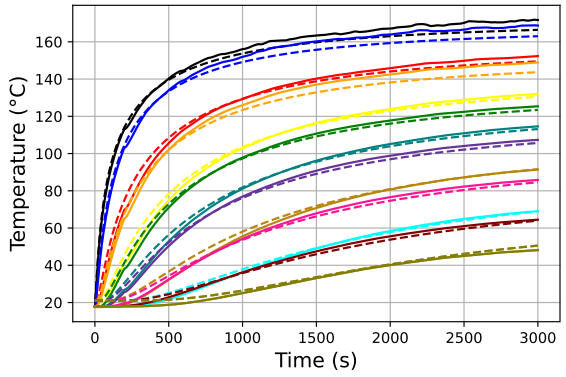

(a) $Y = 5$ cm

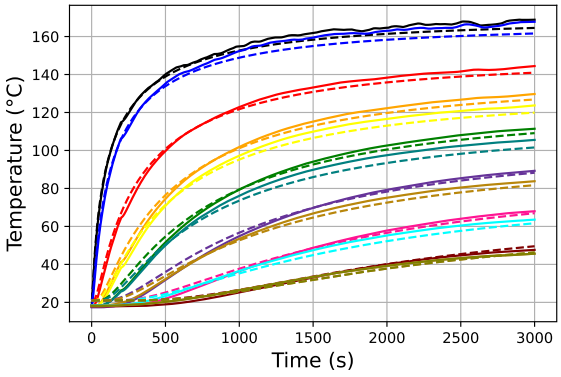

(b) $Y = 3,34$ cm

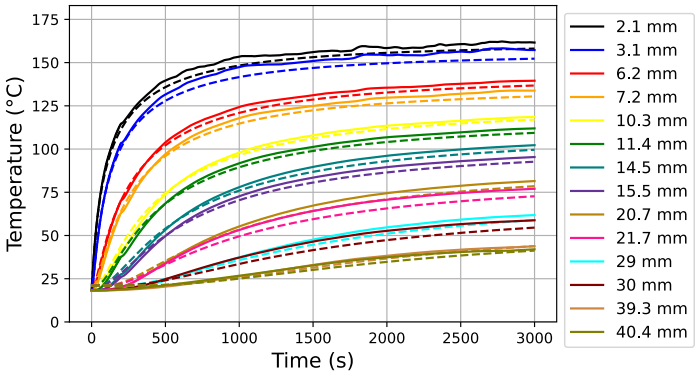

(c) $Y = 1,67$ cm

Fig. A.16. Comparison of the numerical and experimental temperatures obtained for experiment 3, presented in Fig. 5.

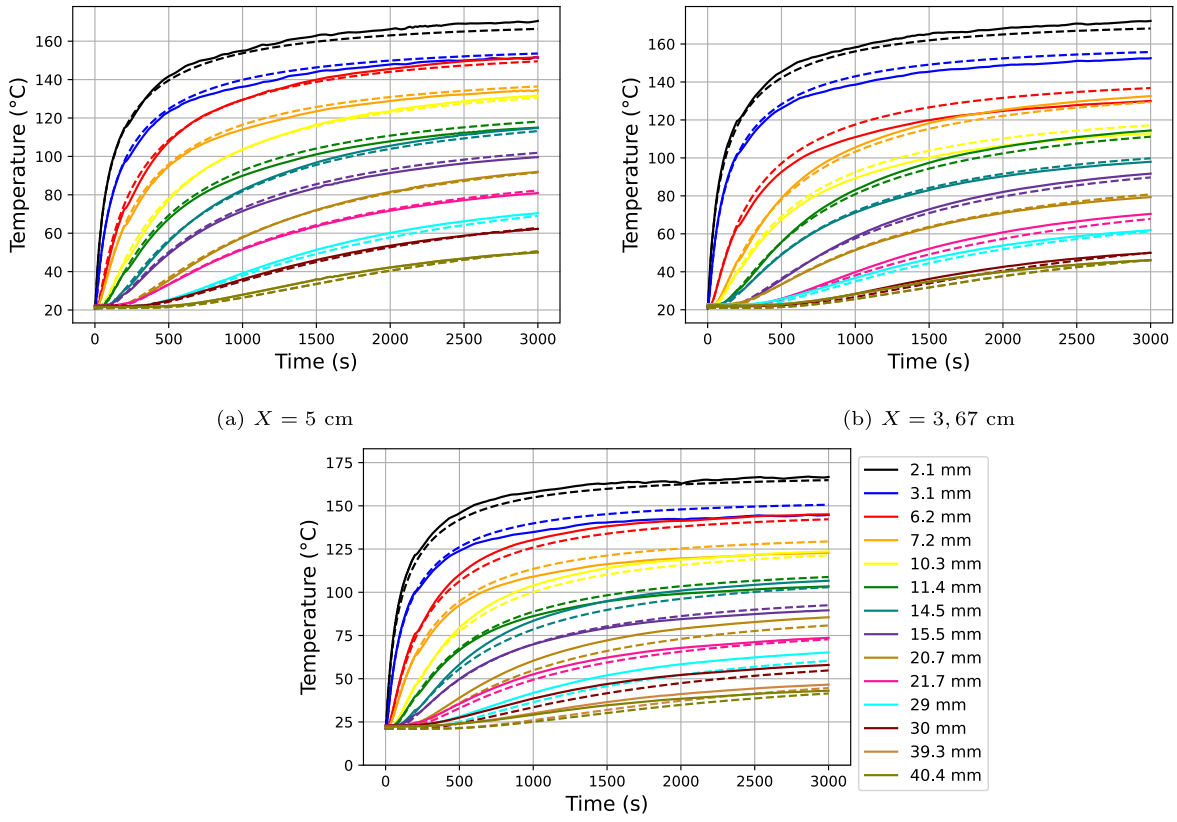

Fig. A.17. Comparison of the numerical and experimental temperatures obtained for experiment 4, presented in Fig. 5.

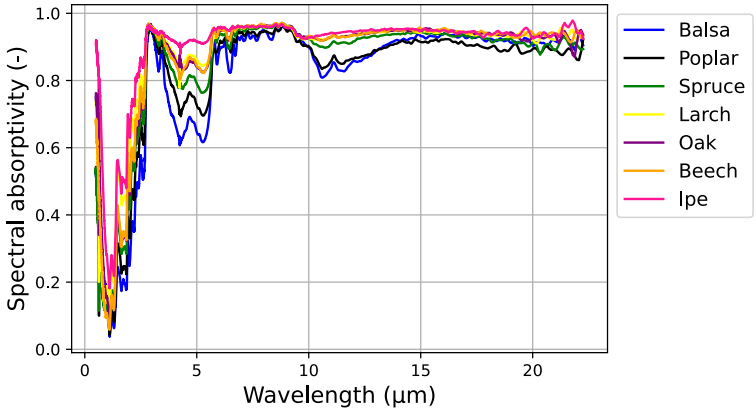

Fig. B.18. Spectral absorptivity of wood for different wood species at room temperature.

References

[1] T. Fateh, T. Rogaume, F. Richard, Multi-scale modeling of the thermal decomposition of fire retardant plywood, Fire Saf. J. 64 (2014) 36–47.

[2] I. Vermesi, M.J. DiDomizio, F. Richter, E.J. Weckman, G. Rein, Pyrolysis and spontaneous ignition of wood under transient irradiation: Experiments and a-priori predictions, Fire Saf. J. 91 (2017) 218–225.

[3] L. Terrei, G. Gerandi, H. Flity, V. Tihay-Felicelli, Z. Acem, G. Parent, P.-A. Santoni, Experimental and numerical multi-scale study of spruce wood degradation under inert atmosphere, Fire Saf. J. 130 (2022) 103598.

[4] F. Richter, G. Rein, A multiscale model of wood pyrolysis in fire to study the roles of chemistry and heat transfer at the mesoscale, Combust. Flame 216 (2020) 316–325.

[5] C. Lautenberger, C. Fernandez-Pello, A model for the oxidative pyrolysis of wood, Combust. Flame 156 (8) (2009) 1503–1513.

[6] O. Authier, M. Ferrer, G. Mauviel, A.-E. Khalfi, J. Lede, Wood fast pyrolysis: comparison of lagrangian and eulerian modeling approaches with experimental measurements, Ind. Eng. Chem. Res. 48 (10) (2009) 4796–4809.

[7] H.R. Baum, A. Atreya, A model of transport of fuel gases in a charring solid and its application to opposed-flow flame spread, Proc. Combust. Inst. 31 (2) (2007) 2633–2641.

[8] C. Di Blasi, Physico-chemical processes occurring inside a degrading two-dimensional anisotropic porous medium, Int. J. Heat Mass Transfer 41 (24) (1998) 4139–4150.

[9] J. Larfeldt, B. Leckner, M.C. Melaaen, Modelling and measurements of heat transfer in charcoal from pyrolysis of large wood particles, Biomass Bioenergy 18 (6) (2000) 507–514.

[10] W.C. Park, A. Atreya, H.R. Baum, Experimental and theoretical investigation of heat and mass transfer processes during wood pyrolysis, Combust. Flame 157 (3) (2010) 481–494.

[11] U. Sand, J. Sandberg, J. Larfeldt, R.B. Fdhila, Numerical prediction of the transport and pyrolysis in the interior and surrounding of dry and wet wood log, Appl. Energy 85 (12) (2008) 1208–1224.
[12] C. Fairbridge, R. Ross, S. Sood, A kinetic and surface study of the thermal decomposition of cellulose powder in inert and oxidizing atmospheres, J. Appl. Polym. Sci. 22 (2) (1978) 497–510.
[13] B.M. Wagenaar, W. Prins, W. van Swaaij, Pyrolysis of biomass in the rotating cone reactor: modelling and experimental justification, Chem. Eng. Sci. 49 (1994) 5109–5126.
[14] M.J. Antal Jr., W.S. Mok, G. Varhegyi, T. Szekely, Review of methods for improving the yield of charcoal from biomass, Energy Fuels 4 (3) (1990) 221–225.
[15] K.A. Murty, P.L. Blackshear Jr., Pyrolysis effects in the transfer of heat and mass in thermally decomposing organic solids, in: Symposium (International) on Combustion, Vol. 11, Elsevier, 1967, pp. 517–523.
[16] C. Di Blasi, Modeling and simulation of combustion processes of charring and non-charring solid fuels, Prog. Energy Combust. Sci. 19 (1) (1993) 71–104.
[17] D. Cancellieri, E. Innocenti, V. Leroy-Cancellieri, Wingpyro: A software platform for kinetic study of forest fuels, Fire Saf. J. 58 (2013) 103–111.
[18] C.A. Koufopanos, A. Lucchesi, G. Maschio, Kinetic modelling of the pyrolysis of biomass and biomass components, Can. J. Chem. Eng. 67 (1989) 75–84.
[19] R. Font, A. Marcilla, J. Devesa, E. Verdú, Gas production by almond shell pyrolysis at high temperature, J. Anal. Appl. Pyrolysis 28 (1) (1994) 13–27.
[20] F. Thurner, U. Mann, Kinetic investigation of wood pyrolysis, Ind. Eng. Chem. Process Des. Dev. 20 (3) (1981) 482–488.
[21] T. Fateh, T. Rogaume, J. Luche, F. Richard, F. Jabouille, Kinetic and mechanism of the thermal degradation of a plywood by using thermogravimetry and fourier-transformed infrared spectroscopy analysis in nitrogen and air atmosphere, Fire Saf. J. 58 (2013) 25–37.
[22] C. Di Blasi, Modeling chemical and physical processes of wood and biomass pyrolysis, Prog. Energy Combust. Sci. 34 (1) (2008) 47–90.
[23] C. Branca, C. Di Blasi, Global interinsic kinetics of wood oxidation, Fuel 83 (1) (2004) 81–87.
[24] C. Branca, C.D. Blasi, Kinetics of the isothermal degradation of wood in the temperature range 528–708 K, J. Anal. Appl. Pyrolysis (2003) 13.
[25] S. Benkorichi, T. Fateh, F. Richard, J.-L. Consalvi, A. Nadjai, Investigation of thermal degradation of pine needles using multi-step reaction mechanisms, Fire Saf. J. 91 (2017) 811–819.
[26] H. Flity, M. Abdo, L. Terrei, Z. Acem, R. Mehaddi, P. Lardet, G. Parent, 3D-modeling of thermal degradation of spruce wood under inert atmosphere, Fire Saf. J. 141 (2023) 103979.
[27] A. Mariam, H. Flity, L. Terrei, A. Zoulalian, R. Mehaddi, P. Girods, Y. Rogaume, An alternative wood pyrolysis model based on tga and cone calorimeter tests, Thermochim. Acta 731 (2024) 179646.
[28] J. Adánez, L.F. de Diego, F. García-Labiano, A. Abad, J.C. Abanades, Determination of biomass char combustion reactivities for fbc applications by a combined method, Ind. Eng. Chem. Res. 40 (20) (2001) 4317–4323.
[29] C. Branca, C. Di Blasi, Global kinetics of wood char devolatilization and combustion, Energy Fuels 17 (6) (2003) 1609–1615.
[30] C. Di Blasi, F. Buonanno, C. Branca, Reactivities of some biomass chars in air, Carbon 37 (8) (1999) 1227–1238.
[31] A.M. Janse, H.G. de Jonge, W. Prins, W.P. van Swaaij, Combustion kinetics of char obtained by flash pyrolysis of pine wood, Ind. Eng. Chem. Res. 37 (10) (1998) 3909–3918.
[32] G. Várhegyi, E. Mészáros, M.J. Antal, J. Bourke, E. Jakab, Combustion kinetics of corncob charcoal and partially demineralized corncob charcoal in the kinetic regime, Ind. Eng. Chem. Res. 45 (14) (2006) 4962–4970.
[33] L. Terrei, Z. Acem, V. Georges, P. Lardet, P. Boulet, G. Parent, Experimental tools applied to ignition study of spruce wood under cone calorimeter, Fire Saf. J. 108 (2019) 102845.
[34] T. Kashiwagi, T. Ohlemiller, K. Werner, Effects of external radiant flux and ambient oxygen concentration on nonflaming gasification rates and evolved products of white pine, Combust. Flame 69 (1987) 331–345.
[35] L. Shi, M.Y.L. Chew, Experimental study of woods under external heat flux by autoignition, J. Therm. Anal. Calorim. 111 (2) (2013) 1399–1407.
[36] V. Babrauskas, W.J. Parker, Ignitability measurements with the cone calorimeter, Fire Mater. 11 (1) (1987) 31–43.
[37] K.-C. Tsai, Orientation effect on cone calorimeter test results to assess fire hazard of materials, J. Hazard. Mater. 172 (2–3) (2009) 763–772.
[38] A. Bartlett, R. Hadden, L. Bisby, B. Lane, Auto-Extinction of Engineered Timber: The Application of Firepoint Theory, Royal Holloway College, Nr Windsor, UK, 2016.
[39] R. Emberley, T. Do, J. Yim, J.L. Torero, Critical heat flux and mass loss rate for extinction of flaming combustion of timber, Fire Saf. J. 91 (2017) 252–258.
[40] L. Terrei, Z. Acem, P. Lardet, P. Boulet, G. Parent, Study of wood self-extinguishment with a double sliding cone calorimeter, Fire Saf. J. 122 (2021) 103316.
[41] J.I. Cuevas, A. Guibaud, C. Maluk, J.L. Torero, Understanding flame extinction in timber under external heating using high-activation energy asymptotics, Combust. Flame 235 (2022) 111645.
[42] H. Flity, Y. Jannot, L. Terrei, P. Lardet, V. Schick, Z. Acem, G. Parent, Thermal conductivity parallel and perpendicular to fibers direction and heat capacity measurements of eight wood species up to 160 ° c, Int. J. Therm. Sci. 195 (2024) 108661.
[43] P. Boulet, G. Parent, Z. Acem, A. Collin, M. Försth, N. Bal, G. Rein, J. Torero, Radiation emission from a heating coil or a halogen lamp on a semitransparent sample, Int. J. Therm. Sci. 77 (2) (2014) 223–232.
[44] L. Terrei, Z. Acem, V. Marchetti, P. Lardet, P. Boulet, G. Parent, In-depth wood temperature measurement using embedded thin wire thermocouples in cone calorimeter tests, Int. J. Therm. Sci. 162 (2021) 106686.
[45] Y. Jannot, A. Degiovanni, An improved model for the parallel hot wire: Application to thermal conductivity measurement of low density insulating materials at high temperature, Int. J. Therm. Sci. 142 (2019) 379–391.